Dehydration of ethyl lactate over alkaline earth phosphates: Performances, effect of water on reaction pathways and active sites

E. Blanco, C. Lorentz, P. Delichere, L. Burel, M. Vrinat, J.M.M. Millet, S. Loridant*

Institut de Recherches sur la Catalyse et l'Environnement de Lyon, IRCELYON, CNRS-Université Claude Bernard Lyon 1, 2 av. Einstein, F-69626 Villeurbanne Cedex, France

A B S T R A C T

In this work, alkaline earth phosphates have been prepared by co-precipitation and evaluated in gas phase dehydration of ethyl lactate to acrylic acid and ethyl acrylate. These solids, which were previously shown to be active for the dehydration of lactic acid, appeared more efficient. Indeed, it was shown that the decarbonylation/decarboxylation route leading to acetaldehyde was strongly inhibited compared to conversion of lactic acid and molar selectivity values to dehydration products reaching 87% were obtained. Furthermore, it was shown that the deactivation of the catalysts could strongly be slowed by addition of water vapor to the feed. The reaction pathways have been studied in the presence and absence of water and it was shown that acrylic acid was mainly formed by a simultaneous dehydration/hydrolysis reaction. The characterization of the catalysts surface from the results of XPS, cross polarization NMR, DRIFT and TEM showed the presence of a surface amorphous layer containing POH species. *In situ* DRIFT measurements have revealed that formation of POH groups was favored under water vapor and that these species interacted with reactants or reaction products at the reaction temperature.

© 2015 Elsevier B.V. All rights reserved.

1. Introduction

Acrylic acid (AA) is a platform molecule used as a building block to produce acrylate polymers and plastics [1]. Its production has grown 4%/year between 2006 and 2011 reaching 4.2 Mt in 2011 and was predicted to increase about 5% per year between 2012 and 2017 [2]. AA is currently produced by catalytic oxidation of propylene using a two-step process. However, it is widely affected by the propylene price as it represents only 2% of its global consumption [1]. An alternative route to produce AA is therefore required especially in the context of commitment to environment-friendly catalytic processes. A first possibility that has been studied in our laboratory could be the dehydration of glycerol to acrolein [3–5] with its subsequent oxidation to AA. It could also correspond to a one step dehydration of lactic acid (LA). This important platform molecule, which can be yielded by sugar fermentation [6] but also from lignocelluloses [6] and glycerol dehydrogenation [7] has gained attention in recent years [1]. However, AA is rarely obtained selectively from LA because of easy decarbonylation/decarboxylation leading to acetaldehyde (A) and CO_x [8–10]. High yields of acrylic acid were obtained using modified zeolites [11–16] but they suffered from coking and probable hydrothermal instability.

Other efficient catalysts for LA dehydration are sulphates [17], alkaline earth phosphates [18–21] and hydroxyapatites [22–24]. Recently, we have shown that selective alkaline earth phosphates contained mostly acidic and basic sites with similar weak strength. Furthermore, a correlation between the selectivity value to acrylic acid and the acid–base balance was clearly established [21]. Later, another correlation was reported over hydroxyapatites with a volcano curve in the AA production rate and an optimal acid–base balance of 4 [20]. A similar cooperative acid–base catalysis was suggested and a reaction scheme involving POH and M^{2+} pairs was proposed.

Alkyl lactates are easier to vaporize and less polymerisable than lactic acid. Their ester functions that are less reactive limit decarbonylation/decarboxylation reactions. The interest in use of alkyl lactate instead of lactic acid as reactant to reach higher AA selectivity has been previously illustrated for $Ca_3(PO_4)_2 - Ca_2(P_2O_7)$ (50/50 wt%) mixture [18]. The highest AA molar selectivity was found for ethyl lactate (79%), followed by methyl lactate (75%) and lactic acid (54%). Moreover, the use of alkyl lactates could simplify the separation and purification process and reduce production costs [25] even if it would imply recycling of co-produced alcohols. In that regard, additional molecules of alkyl lactates could be produced by reaction of recycled alcohols with ammonium lac-

tate obtained by fermentation [26]. Dehydration of methyl lactate to methyl acrylate and acrylic acid over silica supported sodium phosphates was investigated in a fixed-bed continuous flow reactor [25]. The highest molar selectivity to dehydration products (52%) obtained for NaH_2PO_4/SiO_2 catalyst at 380 °C was assumed to be related to the acidity and the amount of POH groups at the end of polyphosphate chains formed during calcination.

In this paper, the catalytic performances of different alkaline earth phosphates in dehydration of ethyl lactate (EL) to ethyl acrylate (EA) and AA were determined and compared to the results obtained for conversion of lactic acid [21]. As ethyl lactate is hydrolysable, different routes depending on the reaction conditions can lead to AA (Fig. 1). Indeed, it can be formed by (i) direct hydrolysis of EA formed by dehydration of EL, (ii) simultaneous dehydration/hydrolysis or (iii) dehydration of LA consecutively to the hydrolysis of EL. Hence, it was essential for further developments to determine which of these pathways was taking place and specific studies have been conducted to answer the question. Furthermore, the influence of the water partial pressure on the catalytic properties and on the reaction mechanisms to dehydration products has been investigated. Finally several characterization techniques like XPS, $(^1H)–^{31}P$ NMR, $^{31}P–^{31}P$ NMR, TEM, DRIFT and in situ DRIFT measurements have been used to identify the active sites and to study the effect of water vapor partial pressure on them.

2. Experimental part

2.1. Catalysts preparations

Alkaline earth orthophosphates (MOP), pyrophosphates (MPP) and hydroxyapatites (MPOH) were synthesized by co-precipitation of phosphorus and M metal salts according to protocols previously described [21]. Several solids were obtained from sodium containing precursors ($Na_4P_2O_7$, Na_2HPO_4) and residual Na was detected [21]. This was specified in their labeling: for instance, calcium pyrophosphate containing residual Na was noted CaPP-Na instead of CaPP for the free Na compound.

2.2. Catalysts characterization

X-ray photoelectron experiments were carried out in a Kratos Axis Ultra DLD spectrometer. The base pressure in the analysis chamber was lower than 5×10^{-8} Pa. The spectra were recorded using the Al Kα X-ray radiation (1486.6 eV), with pass energy of 20 eV and spot size aperture of 300×700 μm. As the samples were insulating, charge neutralizer was used and the binding energies were calibrated using the C 1 s band at 284.6 eV. The O 1 s level was decomposed into individual components after Shirley background subtraction using symmetric line-shape with a Gaussian/Lorentzian product form (GL30). The full width at half maximum values were fixed at 1.4 eV ± 0.1 eV for the O 1 s major component and 1.75 eV ± 0.15 eV for the O 1 s minor component.

$(^1H)–^{31}P$ CP MAS NMR experiments were carried out at 9.4 Tesla on a Bruker DSX400 spectrometer operating at 162.0 MHz. Samples were spun at 10 KHz on a 4 mm triple HXY probe. The spectra were recorded at 10 KHz spinning frequency with a contact time $(^1H)–^{31}P$ of 2 ms over a spectral range of 300 ppm. Recycle delays were set to 40 s and 512 scans were achieved. All ^{31}P chemical shifts were referenced to H_3PO_4 85% (0 ppm). Double quantum ^{31}P NMR experiments were carried out at 11.4 T, an RF field of 105 KHz, a recycle delay of 60 s on a Bruker AVANCE III spectrometer operating at a Larmor frequency of 202.4 MHz. Samples were spun at 15 KHz in a commercial 2.5 mm MAS probe at room temperature and chemical shifts were referenced to H_3PO_4 in aqueous solution (85 wt%). The compensated C7 (Post-C7) pulse sequence

was applied to get through space single quantum–double quantum correlations experiments [27]. Double quantum excitation and recovery time were set to 380 μs. Quadrature detection in the f1 dimension was achieved by the hypercomplex approach. For each t1 increment, 16 transients were accumulated and a total of 128 increments were collected to yield a 2D DQ spectrum. DQ experiments were optimized on a $Zn_2P_2O_7$ reference.

TEM images were achieved with a JEOL 2010 microscope. The acceleration voltage was 200 kV with LaB_6 emission current and the point resolution was 0.19 nm. Before measurements, a dispersion of catalyst crushed in ethanol was deposited on standard holey carbon-covered copper TEM grids. In situ DRIFT spectra were achieved with a Nicolet 6700 FTIR spectrometer (Thermo Scientific) equipped with Praying Mantis™ High Temperature Reaction Chamber (Harrick, model HVC-DRP-4). The CaF_2 windows used for the experiments were heated at 70–80 °C with external water system to avoid condensation. TGA/DTA measurements of used catalysts were achieved under air flow up to 800 °C with a SETARAM TG12 apparatus to characterize the organic matter deposited over catalysts during reaction. NH_3 and CO_2-TPD measurements were achieved using a protocol previously described [21].

2.3. Catalytic testing

Gas phase dehydration of ethyl lactate (EL) or lactic acid (LA) was conducted in a fixed bed reactor at atmospheric pressure. Pure or 20% by weight aqueous solution of reactant was fed using a 307HPLC pump (Gilson) vaporized at 160–170 °C with an in house system and diluted with N_2 before entering the reactor. The vaporization temperature was previously determined from liquid vapor equilibrium simulated by the ProSIM software. Before addition of the vaporized solution, the reactor was heated at the reaction temperature under N_2. After trapping at −20 °C for testing with pure EL and −4 °C for testing with aqueous solution of reactant, the condensed products (mainly ethyl acrylate (EA), acrylic acid (AA), acetaldehyde (A), propionic acid (PA), lactic acid (LA)) were analyzed off-line with a GC-2014 chromatograph (Shimadzu) equipped with AOC-20i auto-injector, ZB-WAXplus (30 m, 0.32 mm) column and FID detector, while gas products, mainly CO, CO_2 and N_2 were analyzed on line with the same chromatograph but using sampling valve, Carboxen1000 column and TCD detector.

The conversion value was varied by changing the contact time defined by:

$$\text{Contact time} = \frac{\text{Volume of catalyst}}{\text{Total gas flow rate}} = D(N_2) + 24055$$
$$\times \left(\frac{d(R)}{M(R)} + \frac{d(H_2O)}{18} \right)$$

where, $D(N_2)$ corresponds to the nitrogen volume flow rate at room temperature, $d(R)$ and $d(H_2O)$ to the mass flow rates of liquid reactant and H_2O, respectively and $M(R)$ to the molar mass of reactant.

The formulas used to calculate the conversions, carbon selectivity sets and the products carbon balances were the following:

$$\text{Conversion (\%)} = \frac{\text{moles of reactant fed} - \text{moles of reactant trapped}}{\text{moles of reactant fed}} \times 100$$

$$\text{Carbon selectivity (\%)} = K \times \frac{\text{moles of product}}{\text{moles of reactant converted}} \times 100 \text{ with}$$

$$K = \frac{\text{number of carbons in product}}{\text{number of carbons in reactant}}$$
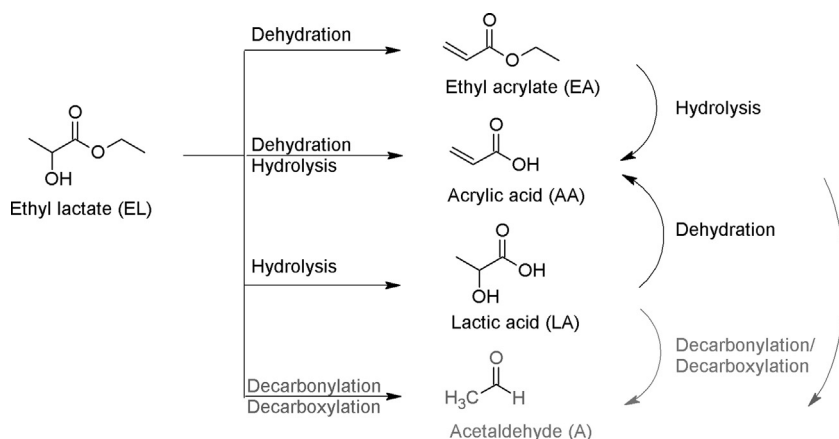
Fig. 1. EL conversion into AA through different pathways.

Products carbon balance $(\%) = \Sigma$ carbon selectivity$(\%)$

$$= \frac{\Sigma K \times \text{ moles of product}}{\text{moles of reactant converted}} \times 100$$

As the desired dehydration products were C_3 and C_5 molecules (respectively AA and EA), molar selectivity sets were also calculated to compare the values with those obtained for lactic acid conversion.

$$\text{Molar selectivity }(\%) = \frac{\text{moles of product}}{\text{moles of reactant converted}} \times 100$$

The accuracy of using this parameter is discussed in Section 3.2.1 by comparison with the carbon selectivity values obtained for CaPOH catalyst.

3. Results

3.1. Characterization of the catalysts

The results of the general characterization of the prepared catalysts have been described in a previous paper [21]. It is important to recall our findings before going into them in depth. X-ray diffraction showed that most of the prepared alkaline earth phosphates contained single crystalline phase. The pyro and orthophosphates exhibited specific surface areas lower than $20\,m^2\,g^{-1}$ whereas, those of hydroxyapatites ranged from 38 to $88\,m^2\,g^{-1}$. Chemical analyses showed sub-stoichiometric bulk M/P ratios that were ascribed to the presence of an additional phosphorus rich amorphous phase. The preliminary study of the surface composition by XPS spectroscopy showed opposite trends depending on the nature of the phosphates: the surfaces of the calcium and barium phosphates were richer in phosphorus than stoichiometry whereas those of strontium phosphates and strontium hydroxyapatites were slightly poorer [21].

To go further into the characterization of the catalysts and to understand the nature of the surface species leading to the surface enrichment into phosphorus, different techniques such as XPS, $(^1H)–^{31}P$ CPMAS NMR, $^{31}P–^{31}P$ NMR, DRIFT and TEM have been used.

The O 1 s XPS spectra of catalysts are plotted in Fig. 2. In most cases, they contained two oxygen components with binding energies around 531.0 and 532.5 eV, respectively attributed to O^{2-} anions present in the bulk structure and to surface hydroxyl groups [28,29]. BaOP-Na appeared as an exception since three components were necessary to correctly fit the O 1 s band. The third component located around 533.5 eV could correspond to OH^- anions in $Ba(OH)_2$ phase [30]. The proportion of the surface hydroxyl

Table 1
XPS O 1 s components and $^1H–^{31}P$ NMR bands of catalysts.

	O 1 s peak		$^1H–^{31}P$ NMR bands (ppm)
	Proportion at 532–533 eV (%)	Proportion at 530–531 eV (%)	
CaPP	24	76	−2.0,−8.3
CaPP-Na	22	78	1.8,−5.7
CaPOH	13	87	2.9
SrPP	24	76	2.7,−5.5
SrPOH	11	89	2.3
SrPOH-Na	13	87	–
BaOP	11	89	0.5
BaOP-Na	12[a]	72[a]	0.6
BaPP	24	76	−1.6, −9.1

[a] A third component was located at 533.5 eV and represented 16% of the O 1 s peak.

band represented 22–24% of the O 1 s signal for pyrophosphates and 11–13% for orthophosphates (Table 1). The higher proportion for pyrophosphates indicated surface hydrolysis of $P_2O_7^{4-}$ groups leading to the formation of HPO_4^{2-} monohydrogenophosphates. Carbonates with one O 1 s band around 532 eV [31] could contribute to the second component. However, they should be a small proportion since only small amounts (<1%) were determined from the C 1 s signal.

$(^1H)–^{31}P$ CPMAS NMR spectroscopy uses the polarization transfer from H to P atoms. Therefore, the corresponding spectra reveal spatial proximity as is the case for POH species for instance. Furthermore, as the crystalline phases detected by XRD were not hydroxylated, this technique was considered as selective to the amorphous phases. The spectra recorded for the different catalysts are provided in Fig. S1 (Supporting information) and their positions on Table 1. For pyrophosphates, two bands were observed suggesting the presence of two types of phosphorus atoms interacting with hydrogen. The bands located between −5.5 and −9.0 ppm could be assigned to Q1(1H) phosphorous site (a Q1 phosphate tetrahedron with one hydroxyl group) and would imply the presence of polyphosphate chains [25,32,33]. However, such a band was not observed for orthophosphates and hydroxyapatites (Table 1) and the double quantum $^{31}P–^{31}P$ NMR measurement achieved on BaOP catalyst revealed only the auto-correlated peak (Fig. S2) suggesting the absence of P—O—P bridging bonds in this catalyst. Hence, the prepared pyrophosphates could contain polyphosphates but not the orthophosphates and hydroxyapatites. The only common feature to all the catalysts was one band located between −2 and 3 ppm (Table 1) that was attributed to HPO_4^{2-} anions. Indeed, $CaHPO_4$ and CaPOH which contain such groups exhibited one band at −2.1 ppm and 2.9 ppm respectively (Fig. S1) in agreement with
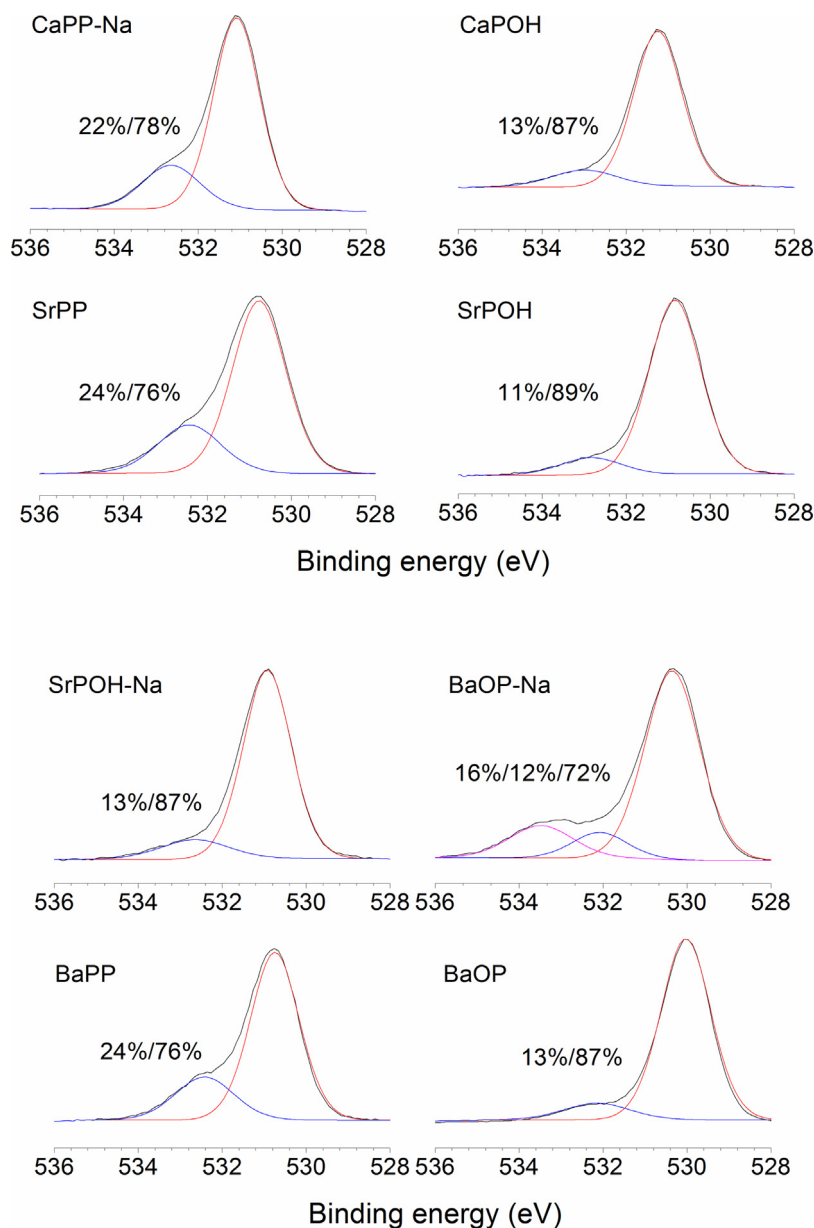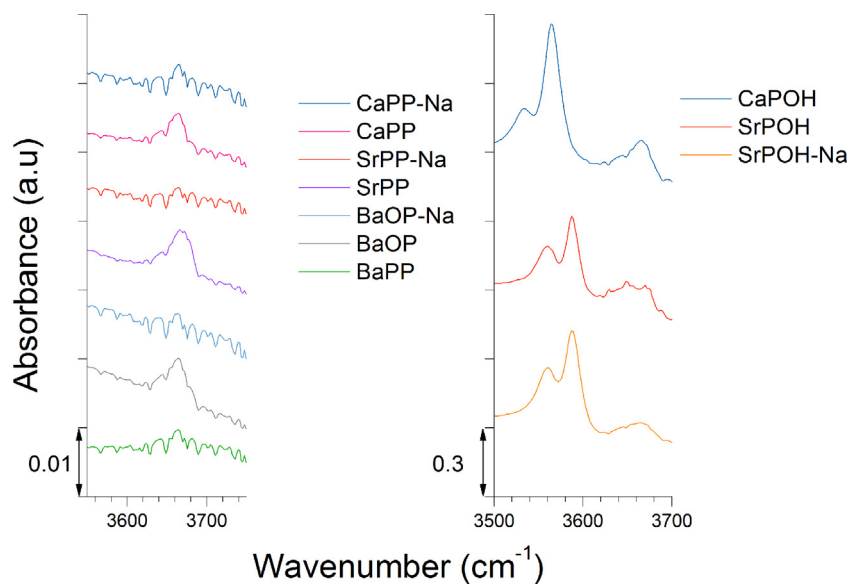
Fig. 2. XPS O 1 s spectra of different alkaline earth phosphates.

data reported in the literature [34–36] and a band around 0 ppm was observed for $Ca_8(HPO_4)_2(PO_4)_4 \cdot 5H_2O$ octocalcium phosphate [37]. However, it is hard to state precisely in which phase HPO_4 entities would be contained since their positions are rather close for the three phases.

Therefore, other techniques characterizing the hydroxyl groups of catalysts were needed. DRIFT spectra of catalysts treated under helium flow at the reaction temperature (380 °C) were achieved and are plotted in Fig. 3. For the hydroxyapatites, stretching vibrations of lattice OH^- anions were located between 3500 and 3600 cm^{-1} [38–41]. Furthermore, one band was observed around 3665 cm^{-1} for most of the catalysts. By analogy with deficient hydroxyapatites [38,40,41], it was ascribed to $\nu(PO-H)$ stretching vibrations of surface species. On the contrary, because no OH stretching vibrations were observed below 3600 cm^{-1} for orthophosphates and pyrophosphates, it was concluded that they did not contain hydroxyapatites. Interestingly, the $\nu(PO-H)$ bands were observed below 3400 cm^{-1} for alkaline earth

hydrogenophosphates [42–46]. This large difference of location could arise from the effect of hydrogen bonds in bulk hydrogenophosphates leading to weakening of PO–H bonds and stretching vibrations at lower wavenumbers. A sharp band at 3676 cm^{-1} attributed to POH groups was also observed for H_3PO_4/Al_2O_3 catalysts [47]. Its intensity increased with increasing phosphorus content up to a limit above which polyphosphates species were formed.

TEM characterization of BaOP and BaPP catalysts has been carried out to find whether these POH species were molecular surface species or present in amorphous phase not detected by XRD. An amorphous phase present as layer of few nanometers and large islands was unambiguously observed at the surface of phosphates crystallites (Fig. 4). This surface phase was quite unstable under electron beam and crystallized quickly into BaHPO$_4$ phase (Fig. S3). Similarly, the presence of an amorphous surface layer 1–2 nm thick over crystalline core of $Ca_5(PO_4)_3OH$ hydroxyapatites was previously reported [48].

Fig. 3. DRIFT spectra of different alkaline earth phosphates and references treated at 380 °C under He. The backgrounds corresponded to the spectrum of KBr in the same conditions.
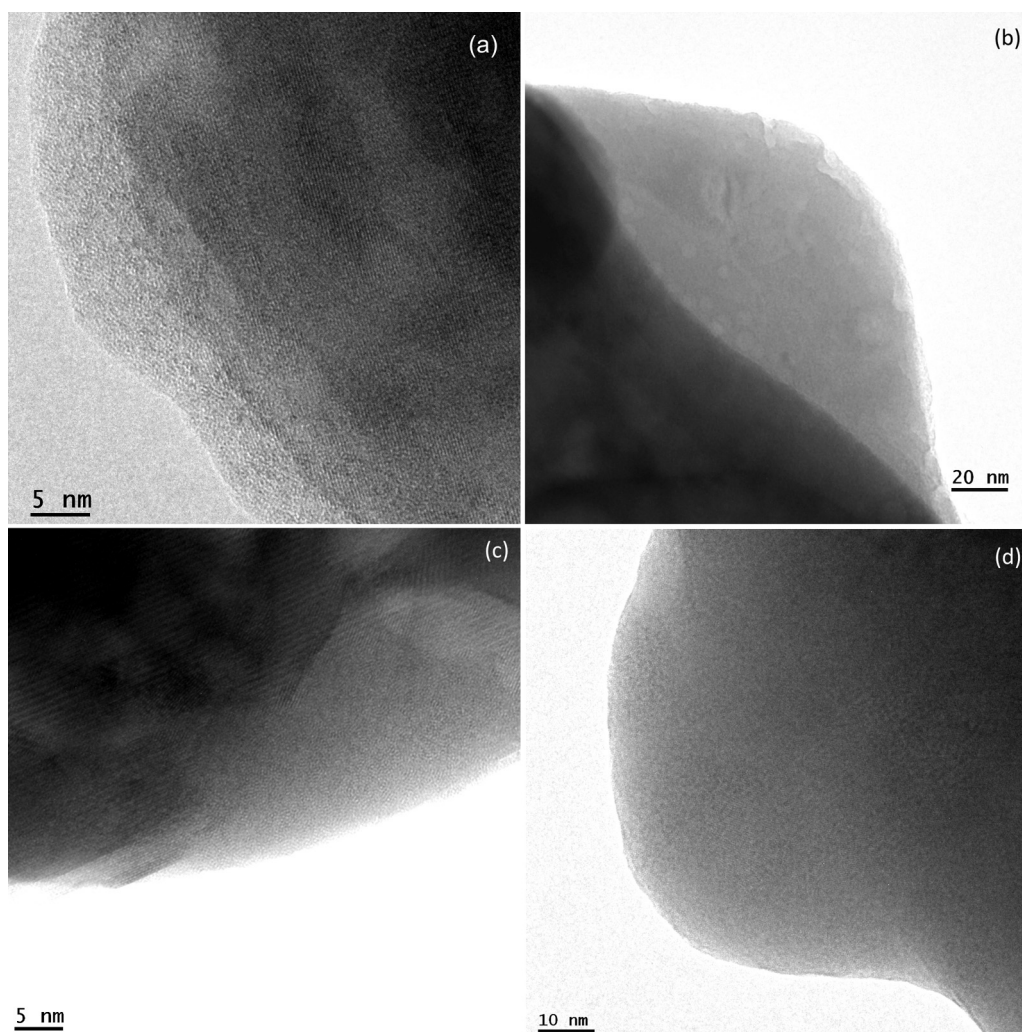
Fig. 4. TEM images of (a and b) BaOP and (c and d) BaPP catalysts.

Table 2
Comparison of the selectivity sets obtained for CaPOH tested at 380 °C under EL/N_2 = 9/91. Contact time of 2.4 s.

Conversion(%)	Carbon selectivity (%)							Sum of selectivity (%)
	EA	AA	EtOH	A	COx	PA	LA	
60	26	21	18	12	11	5	3	96
	Molar selectivity (%)							
	EA	AA	–	A	–	PA	LA	–
	26	35	–	30	–	8	5	104

3.2. Conversion of ethyl lactate

3.2.1. Feed without water

Blank testing was achieved with a feed EL/N_2:9/91 and a total gas flow of 50 mL min^{-1}. Conversion was below 6% at 380 °C, which confirmed that ethyl lactate was much more stable than lactic acid for which conversion of 30% was measured at the same temperature [21].

Catalytic properties of CaPOH catalyst obtained with this feed at 380 °C are reported in Table 2. The sum of carbon selectivity (products carbon balance) was 96% which strengthened the quality of the GC analysis. The main products were EA and AA showing that the dehydration routes (Fig. 1) were the most favorable. Furthermore, the carbon selectivity to EtOH (18%) was two-thirds of the sum of selectivity to to AA, PA and LA (29%) which indicated that EtOH was mainly co-produced with these compounds (2 versus 3 carbon atoms). The carbon selectivity to A and CO$_x$ was 12 and 11% respectively which indicated that the decarbonylation/decarboxylation route was secondary. The minor by-products were PA (5%) which can be formed by hydrogenation (after decarboxylation reaction providing H$_2$ [49]) and of AA or of LA (3%) formed by EL hydrolysis (Fig. 1). For better comparison of the different routes, molar selectivity values were calculated. The sum of the selectivity values was slightly higher than 100% which could arise from overestimation of A selectivity since this product can be formed consecutively from other products. Anyway, it appeared clear that the dehydration routes to EA and AA were majority and that the decarbonylation/decarboxylation one was secondary.

The effect of reaction temperature on catalytic properties was investigated between 350 and 390 °C for this catalyst after a short time on stream (less than 4 h). The evolutions of conversion, products carbon balance and molar selectivity values are plotted with regard to the reaction temperature in Fig. S4. As in the case of LA conversion [21], an optimum of products carbon balance was observed around 370–380 °C with a strong increase (from 76 to 95% between 350 and 370 °C), a plateau and a decrease above 380 °C. The poor carbon balance at 350 °C could reveal limitation of products desorption and/or polymerization. AA selectivity exhibited an optimum of 44% at 370 °C and decreased above this temperature to the benefit of A selectivity. EA selectivity roughly increased reaching 25% at 390 °C. LA selectivity was maximal at 350 °C and decreased above indicating that LA conversion was then activated. Finally, as a temperature of 380 °C was chosen for comparison with LA conversion [21] and as the optimal selectivity in dehydration products was obtained near this value, the following catalytic measurements were achieved at 380 °C.

The best molar selectivity values in dehydration products (EA + AA) measured at 380 °C for different alkaline earth phosphates are gathered in Table 3. Use of molar selectivity allowed comparison with the data obtained for LA conversion in spite of different numbers of carbon atoms (5 instead of 3). Values higher than 63% and reaching 87% for CaPP-Na were obtained which was much higher than for LA conversion on the same catalysts [21]. This improvement was explained by the less reactive carbonyl function of EL compared to LA in agreement with the literature [18]. Hence, the

Table 3
Best selectivity values in dehydration products obtained with different alkaline earth phosphates at 380 °C under EL/N_2 = 9/91 gas feed. Time on stream: 2–4 h.

| Catalyst	Contact time (s)	Conversion (%)	Molar selectivity (%)					
			A	EA	PA	AA	LA	EA + AA
CaPP	1.8	25	23	24	7	50	0	74
CaPP-Na	2.4	15	7	12	11	75	0	87
CaPOH	0.3	28	22	21	13	42	8	63
SrPP	1.4	24	11	27	11	39	7	66
SrPOH	0.7	28	15	23	14	44	4	67
SrPOH-Na	1.0	29	13	19	13	52	0	71
BaOP	1.8	11	7	12	13	68	8	80
BaOP-Na	0.7	8	9	14	13	72	0	86
BaPP	2.4	10	7	17	10	53	8	70

reactant decarbonylation was strongly inhibited compared to LA conversion with A molar selectivity lower than 25%.

All the catalysts strongly deactivated using the reaction feed EL/N_2:9/91. For instance, conversion was damped from 97 to 28% after 30 h for CaPOH and contact time of 2.4 s (Fig. S5a). After thermal treatment for 6 h under air flow at its calcination temperature (500 °C), the catalyst recovered only a part of its initial activity (conversion of 78%). Furthermore, EA and A selectivity values decreased from 28 to 23% and from 32 to 27% respectively. On the other hand, a slight raise of PA, AA and LA selectivity values was observed without complete compensation (Fig. S5b). One explanation for the loss of activity after regeneration could be a decrease in the specific surface area but this remained constant. To explain the difference of catalytic properties, the acid–base properties of the fresh and regenerated CaPOH catalyst have been compared. After regeneration, the surface density of acid sites determined by NH$_3$-TPD remained similar while their strength diminished (Fig. S6). Additionally, weak basic sites were formed as shown by CO$_2$-TPD (Fig. S6). Such modifications of acid base properties could explain both the loss of activity and modifications of selectivity after regeneration. Finally, the TGA/DTA curves of spent CaPOH catalyst (Fig. S7a) showed a weight loss of 19% between 376 and 473 °C with two exothermic peaks revealing that deactivation might be due to the formation of two types of coke. It also demonstrated that almost all the coke formed was burnt after regeneration at 500 °C and that the loss of activity arose from modifications of acid–base properties.

3.2.2. Effect of water on catalytic properties

CaPOH was shown to suffer from a strong deactivation during EL conversion contrarily to LA conversion [21]. However, the feed contained 66% of water in the latter case. It was thus interesting to study the effect of water on EL conversion and this has been done on both CaPOH and BaOP catalysts.
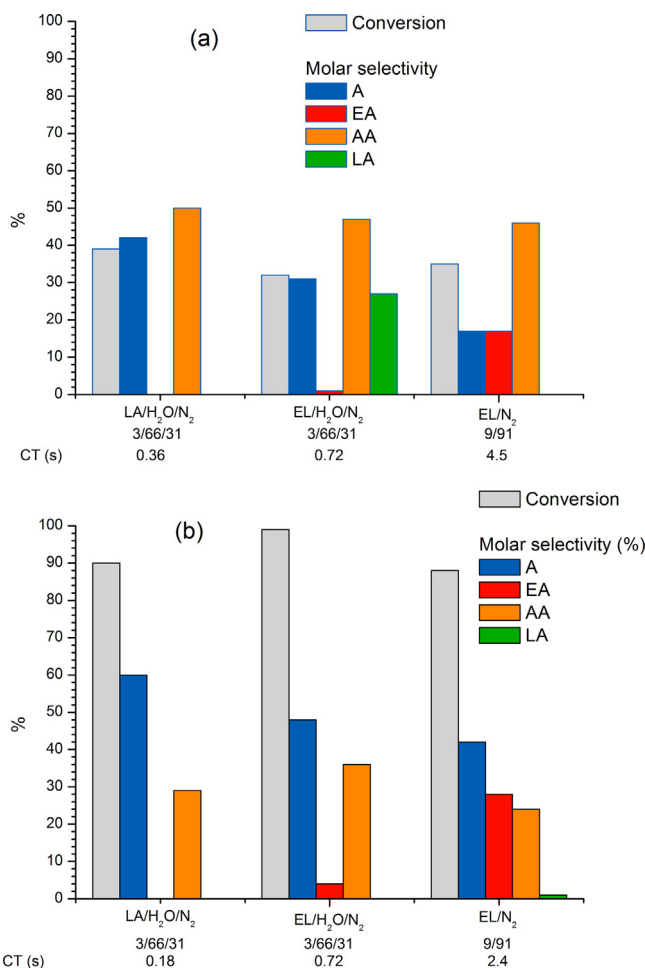
The evolutions of conversion with the mass of EL fed to mass of CaPOH catalyst ratio is shown in Fig. 5a for different water partial pressures. This ratio was chosen to allow comparison of the data. The conversion value measured adding only 1% of water was similar to the one without water. However, higher initial conversion was reached with 9% of water while the deactivation rate remained elevated. Another experiment has been carried out at 380 °C feeding EL with a high proportion of water (66%). The contact time was strongly decreased (0.36 instead of 2.4 s) in order to get conversion lower than 100%. Indeed, water addition favors EL hydrolysis to AL and EtOH and as AL is more reactive, EL conversion was much higher than without water. As shown in Fig. 5a, the stability of CaPOH catalyst was in this case much higher. From TGA analysis of the spent catalysts (Fig. S7b), a weight loss of 17.5% was calculated, which was close to the value measured without water (19%, Fig. S7a). As a reactant flow rate 6 times higher (contact time of 0.36 s instead of 2.4 s) was used for a same testing duration, it means that the coking rate was much smaller adding 66% of water, which explained
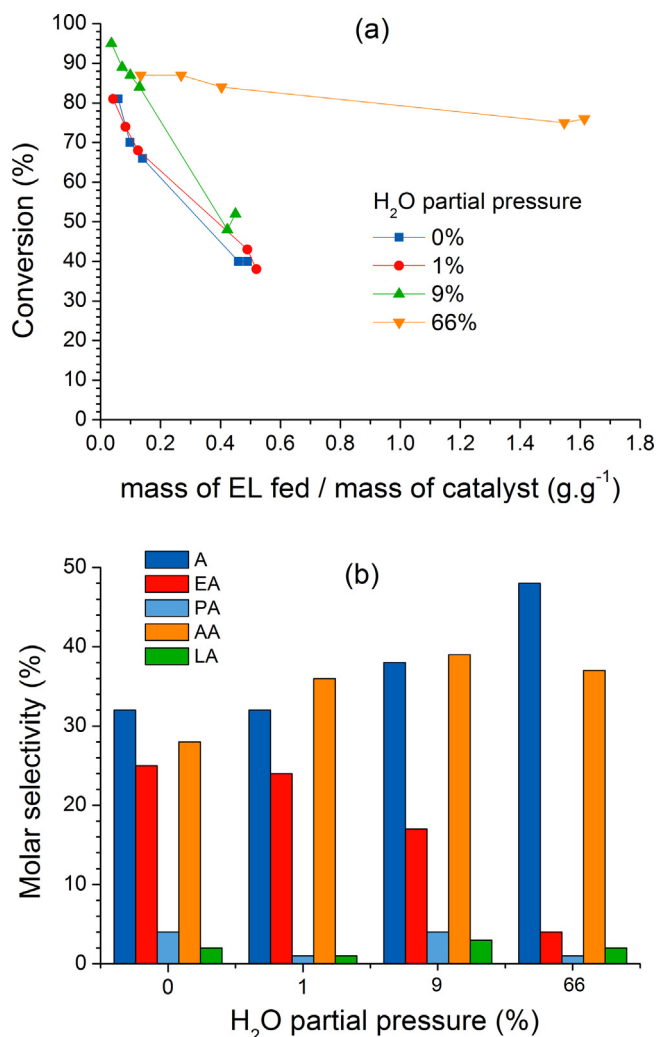
Fig.5. (a) Evolution of EL conversion with the mass of EL fed/mass of CaPOH ratio (b) and selectivities at iso-conversion (81–84%) obtained for CaPOH tested under different water partial pressure at 380 °C. P$_{EL}$ 9%, contact time: 2.4 s except for water partial pressure of 66% (0.36 s), testing duration: 27–30 h. A: Acetaldehyde, EA: ethyl acrylate, PA: propionic acid, AA: acrylic acid, LA: lactic acid.


Fig. 6. Comparison of catalytic performances for LA and EL conversion at 380 °C using (a) BaOP and (b) CaPOH catalysts. Time on stream: 2–4 h. A: Acetaldehyde, EA: ethyl acrylate, PA: propionic acid, AA: acrylic acid, LA: lactic acid. CT: contact time.

the stability improvement observed. This improvement could arise from easier desorption of products limiting polymerization process or modification of sites leading to coke formation. Furthermore, the corresponding DTA curve did not contain the peak at 380 °C suggesting that deactivation was caused by soft coke burning at this temperature (Fig. S7a).

The effect of water addition on the CaPOH molar selectivity sets is shown in Fig. 5b. The data were compared at iso-conversion (81–84%). Addition of water led to a strong decrease in EA selectivity mainly to the benefit of A and to a lesser extent, of AA suggesting that water favors EL and EA hydrolysis followed by decarbony(xy)lation reaction (Fig. 1). An opposite evolution of EA and A was also observed for BaOP catalyst (Fig. 6a) which presented high LA selectivity (27%) under feed containing 66% of water clearly evidencing that EL was hydrolyzed in these reaction conditions. However, the LA selectivity values obtained for CaPOH and BaOP cannot be compared since the conversions were significantly different (see part 3.2.4). Finally, the catalytic performances obtained with the two catalysts for LA and EL conversion were compared at 380 °C for feed composition LA(EL)/H$_2$O/N$_2$ = 3/66/31%. The data plotted in Fig. 6b for CaPOH and compared at conversion of 90–98% indicated that dehydration products were formed in higher proportion using EL

(40% instead of 29%). For BaOP catalyst, the selectivity values were compared at conversion around 35% (Fig. 6a). The selectivity to A was significantly decreased using EL and a high selectivity to LA was obtained contrarily to CaPOH.

3.2.3. Reaction pathway to dehydration products

As presented in Fig. 1, AA can be obtained by three different ways: EL can be hydrolyzed into LA which can then dehydrate, EL can also firstly dehydrate leading to EA that can be then hydrolyzed and finally, AA can be obtained by direct dehydration/hydrolysis (no desorption between the two reactions). In that respect, Hong et al. proposed that AA was mainly formed by such a direct route in the case of methyl lactate (ML) diluted with water (50:50) [18].

The selectivity-conversion curve of CaPOH catalyst under feed without water presented in Fig. 7a allowed the main reaction pathways to be determined. Different conversion values were obtained by varying the contact time between 0.2 and 2.4 s. EA selectivity increased from 12 to 24% when conversion was raised from 13 to 33% and then remained almost constant to reach 28% at 88% conversion. As EA selectivity did not decrease with conversion, one can conclude that AA was not formed consecutively from this primary product. LA selectivity that was maximal at low conversion decreased to 2–4% at high conversion. This decrease occurred mainly for the benefit of AA selectivity indicating that LA was mainly dehydrated into AA. Hence, AA selectivity slightly increased at low conversion (up to ca 45% at 35% conversion) and then fell to
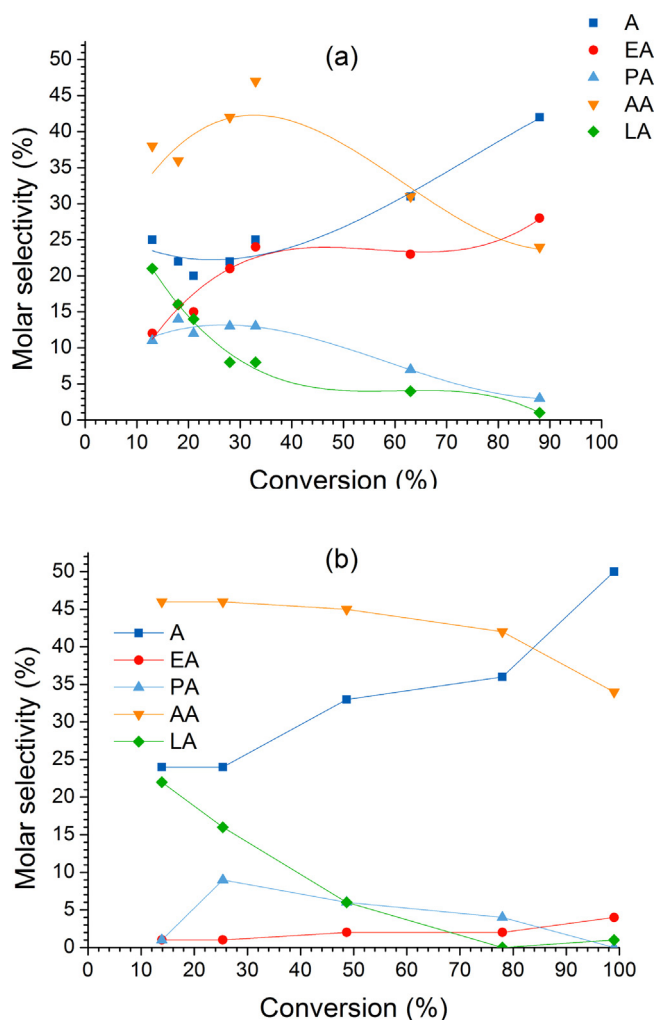
Fig. 7. Selectivity–Conversion curves for CaPOH catalyst tested at 380 °C under (a) EL/N$_2$ = 9/91 and (b) EL/H$_2$O/N$_2$ = 9/66/25 gas feed. Contact time: 0.2–2.4 s. Time on stream: 3 h. A: acetaldehyde, EA: ethyl acrylate, AA: acrylic acid, LA: lactic acid.

24% at higher conversion while A rose from 22 to 42%. This indicated that AA could be decomposed at high conversion into A and CO$_x$ (Fig. 1). The fact that the initial AA selectivity value was significantly higher than that for LA suggested that AA was not mainly created by consecutive dehydration of LA but from a direct dehydration/hydrolysis reaction. Finally, the PA selectivity was constant (around 12%) until a conversion of 35% and decreased above indicating that PA could also decompose into A and CO$_x$.

The evolution of products selectivity versus the conversion has been investigated for the same catalyst with feed containing 66% of water in order to determine the influence of water on the reaction pathways (Fig. 7b). AA selectivity remained almost stable at 45–42% up to a conversion of 80% and decreased to 33% at higher conversion for the benefit of EA and A. As observed for feed without water, LA selectivity decreased strongly from 22% to 0% between 16% and 80% of conversion. This loss can be correlated to the increase in A selectivity from 24 to 36% and PA selectivity from 1 to 5%. The fact that AA and LA selectivity values did not oppositely evolve in the presence of a high amount of water suggested that AA was obtained through a single route, which corresponds to the direct dehydration/hydrolysis reaction. As the evolutions of the conversion-AA selectivity curves were different for the two feeds, one could conclude that water has an impact on adsorption or/and reaction mechanism and/or on the nature of active sites. Finally, EA selectivity slightly increased with conversion but remained very

low (maximum of 4% at conversion of 99%) showing the simple dehydration route was then inhibited. Finally, the close LA selectivity values measured for the two feeds (Fig. 7a and b) suggested that EL hydrolysis was similar in both cases.

3.2.4. Effect of water on hydroxylation and identification of active sites

As the reaction mixtures contained H$_2$O already present in the vaporized solution or formed by the dehydration reactions, its specific influence on the POH groups present in overlayers was investigated by DRIFT spectroscopy. For that purpose, the EL partial pressure was kept constant and water was substituted by nitrogen. The DRIFT spectra compared in Fig.8 showed that the intensity of the POH bands was unchanged (CaPOH, SrPOH-Na, SrPP) or increased (CaPP-Na, CaPP, BaPP, BaOP-Na, BaOP) indicating that POH groups present at the surface of the catalysts remained stable or were formed under water vapor. No additional OH stretching vibrations were observed.

At this step, it was important to determine the catalytic role of the POH groups. For that purpose, in situ DRIFT spectra were recorded over time on stream using BaOP and CaPP-Na catalysts that were among the most AA selective ones (Table 2). The bands appearing in the 1300–1450, 1550–1640, 1710–1760 and 2900–3000 cm^{-1} ranges (Fig. 9) were assigned to δ(C—H), v(C=O) of COO— carboxylates, v(C=O) of carboxylic acids or esters and v(C—H) respectively [50]. In parallel, the two bands at 2329–2364 cm^{-1} corresponding to the Fermi doublet of CO$_2$ decreased over time. The disappearance of the CO$_2$ band suggested that EL was decarboxylated during the first minutes of reaction on strong acid sites. However, a key feature was the negative intensity of the v(PO—H) band around 3665 cm^{-1} for the two catalysts evidencing that POH groups were active species in EL conversion i.e., were involved in at least one step of the reaction pathways. The evolutions observed for CaPOH and CaPP catalysts were similar to those of BaOP and CaPP-Na respectively (Fig. S8). In the case of CaPP-Na and CaPP, a band appeared at 3580 cm^{-1} simultaneously indicating that POH groups were then not consumed but interacted via hydrogen bonds leading to softening of their stretching vibrations. As CaPOH and CaPP had the highest selectivity to A (Table 2), the results suggested the absence of any correlation between the spectral evolutions and AA selectivity.

4. Discussion

High selectivity values to AA and EA dehydration products were obtained for different alkaline earth phosphates confirming the interest of using alkyl lactate as a reactant instead of lactic acid [18]. Indeed, the decarboxylation/decarbonylation routes are then limited. For instance, a molar selectivity to A of 7% was measured at 15% of EL conversion with CaPP-Na (Table 3) versus 45% at 25% of LA conversion [21]. The difference is probably less important at high conversion but only CaPOH could be tested at high conversion in this work. In any case, the data obtained for this catalyst confirmed the limitation since the A molar selectivity was 42% at 88% of EL conversion (Fig. 7a) whereas a value of 68% was obtained at complete conversion of LA [21]. The lower conversion values measured for a given contact time of reactant were explained by the higher stability of EL compared to AL. Consequently, alkaline earth phosphates with high surface areas are required to get high yields and productivities.

However, the catalysts suffer from deactivation over time, which was attributed to EA polymerization leading to soft coke formation. Similarly, Al$_2$(SO$_4$)$_3$ and K$_2$HPO$_4$ modified MCM-41 tested for conversion of methyl lactate were shown to deactivate [51]. In the present work, much higher stability was observed after adding
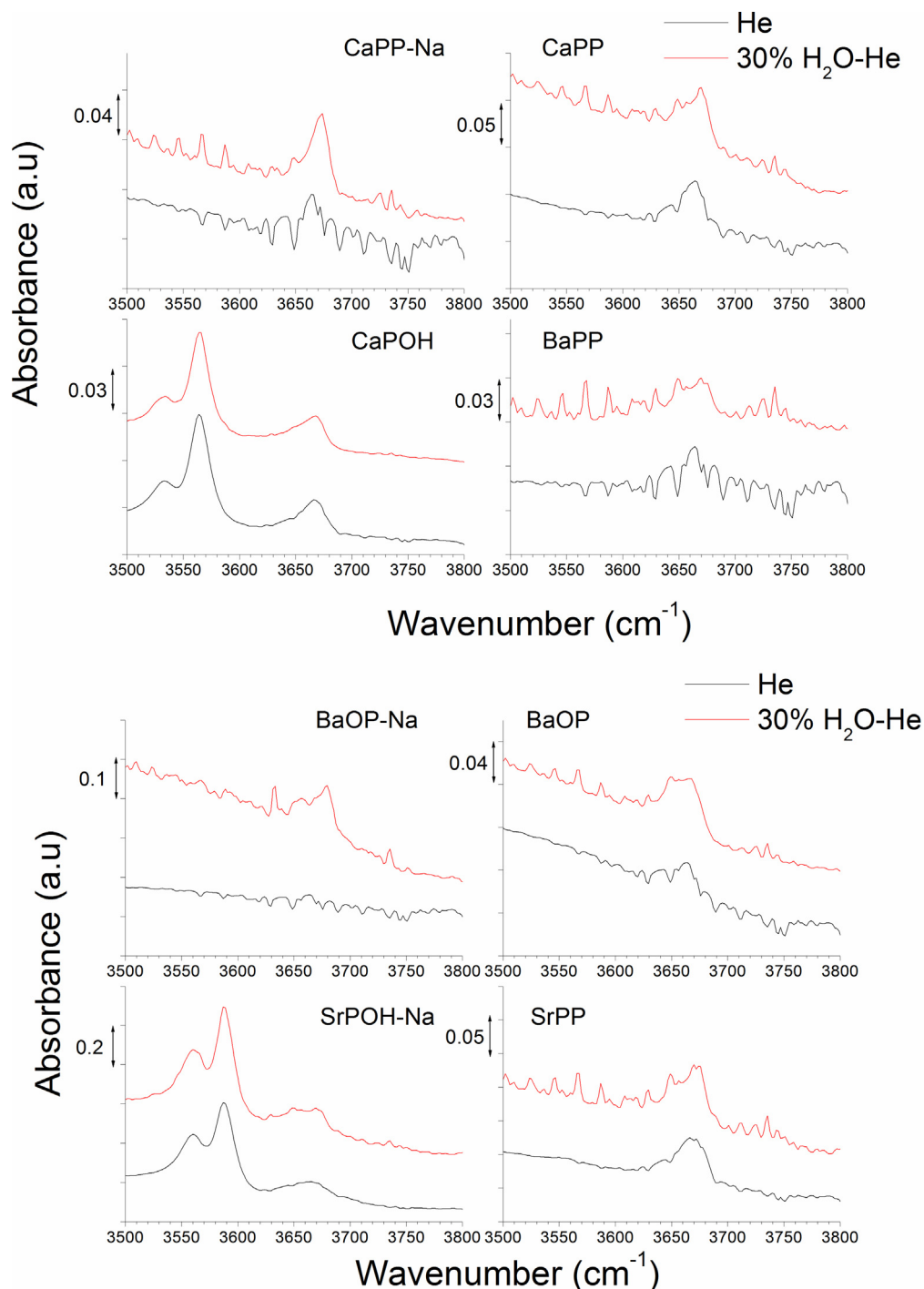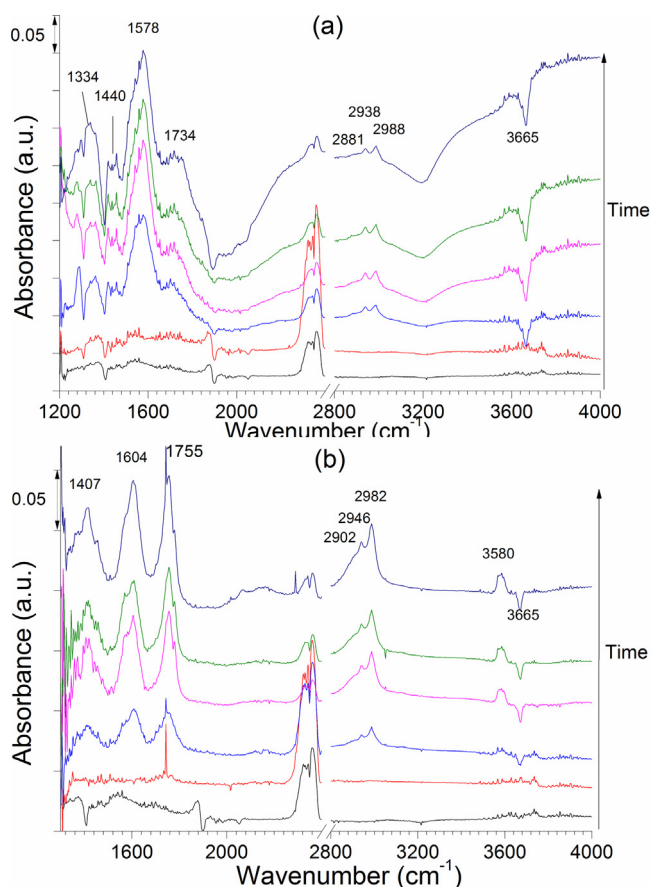
Fig. 8. DRIFT spectra of catalysts at 380 °C under He or 30% H_2O-He flow (30 mL min^{-1}) after 30 min. The background corresponds to the spectrum of KBr in the same conditions.

large amount of water vapor to the feed. Water favors EA hydrolysis into AA and ethanol avoiding both its polymerization (and formation of coke) and its decarbonylation/decarboxylation leading to A (Fig. 1). Therefore, the water partial pressure has to be optimized in order to obtain a good compromise between stability and selectivity to dehydration products.

Furthermore, the conversion-selectivity curves clearly indicate that AA is a primary product formed by a simultaneous dehydration/hydrolysis reaction and not from EA hydrolysis. Without water addition, the AA selectivity depended significantly on the

conversion because it is decomposed at high conversion into A. Consequently, AA selectivity values have to be compared at isoconversion. Close values (42–51%) were measured for five catalysts at conversion of 24–29% (Table 2) in spite of different acid–base balances (2.1 for CaPOH against 1.5 for SrPOH [21]). It means that the acid–base balance did not determine AA selectivity (nor EA + AA) in this case contrarily to LA conversion [21] and could reveal different adsorption modes between EL and LA at the surface of the catalysts.

Surface characterization obtained through combined results of XPS, (^{1}H)–^{31}P NMR, DRIFT and TEM revealed the presence of an

Fig. 9. *in situ* DRIFT spectra of (a) BaOP and (b) CaPP-Na catalysts at 380 °C under feed EL/He = 9/91% (contact time ca 1.7 s) versus time on stream for 2 h. The catalysts were pre-treated under helium flow at 380 °C. The backgrounds correspond to the spectra of the catalysts recorded under He flow at 380 °C.

amorphous surface layer containing POH groups over the alkaline earth phosphates crystallites that made the catalysts more active. Even if the presence of polyphosphates was suggested for the prepared pyrophosphates from (^{1}H)–^{31}P NMR spectra (Fig. S1), ^{31}P–^{31}P NMR spectra recorded for BaOP (Fig. S2) which also contained POH species did not reveal such a phase. Hence, the overlayer observed by TEM (Fig. 3a) could correspond, at least for BaOP catalyst, to an amorphous mono/dihydrogenophosphate phase. *In situ* DRIFT measurements have shown that the surface POH groups were consumed or interacted in reaction conditions. The number of such groups was shown to increase as well as the EL conversion when water is added to the feed confirming they are active sites. Zhang et al. who investigated supported sodium phosphates for dehydration of methyl lactate to methyl acrylate and acrylic acid, proposed that the catalyst efficiency was related to the amount of terminal POH groups present at the end of surface polyphosphate chains [25]. In the present study, it was shown that the number of POH species increased or was maintained under water vapor flow at the reaction temperature whilst at the same time the yield and selectivity to A increased. Therefore, it can be proposed that the POH species contained in the studied catalysts were active but unselective sites for the dehydration reactions. It was previously reported that POH Brønsted acid sites formed by hydrolysis of P—O—P bonds at the surface of vanadyl pyrophosphate catalyst favored strong adsorption of benzaldehyde *via* hydrogen bonding of the carbonyl groups [52,53]. Similarly, POH species present at the surface of alkaline earth phosphates could lead to particular adsorption mode favoring decarbonylation/decarbonylation. We previously proposed that acid–base pairs were active sites for dehydration of LA [21]. Considering the same sites are selective for dehydration of EL would imply that POH species are not involved in such pairs that consequently would be P—O$^-$ and M^{2+} groups.

5. Conclusions

The results obtained in this study showed that alkaline earth phosphates were active and selective catalysts for the dehydration of ethyl lactate into acrylic acid. The catalysts appeared much more selective for acrylic acid than when tested for the dehydration of lactic acid and they also led to ethyl acrylate that can easily be valorized. The data clearly showed that these high selectivities were related to the inhibition of the decarbonylation/decarboxylation reactions. The conversion of ethyl lactate was lower than that of lactic acid because of its higher stability and because of the polymerization of ethyl acrylate at the surface of the catalysts that led to a strong deactivation of catalysts. Addition of large amount of water to the feed limits EA formation, which improves the stability but it also favored the formation of acetaldehyde and reduced the selectivity to dehydration products. Hence the water vapor pressure has to be optimized to obtain the best yields. These results were explained from a mechanistic study achieved under feed containing water or not, which also showed that AA was not mainly formed by hydrolysis of EA or dehydration of LA (formed by hydrolysis) but by an independent dehydration/hydrolysis route.

The characterization of the catalysts revealed the presence of surface layers of amorphous phases of few nanometers lying over crystalline phosphates. These phases, which contain the active sites could correspond to alkaline earth mono/dihydrogenophosphates or polyphosphates. They systematically contained POH groups that were shown to interact with the reactant or reaction products under reaction feed and were thus involved in the reaction pathway. If these species are active, they could correspond to unselective sites since their number increased under water vapor while the selectivity to dehydration products decreased. Further investigations have been undertaken to undoubtedly identify the active and selective sites for EL and LA dehydration reactions. These sites could correspond to acid-base pairs involved in E2 concerted mechanism. In that respect, it can be recalled that a correlation between acrylic selectivity and the acid–base balance has earlier been established for the same catalysts in conversion of lactic acid [18].

Appendix A. Supplementary data

Supplementary data associated with this article can be found, in the online version, at http://dx.doi.org/10.1016/j.apcatb.2015.07.005

References

[1] P. Mäki-Arvela, I.L. Simakova, T. Salmi, D.Y. Murzin, Chem. Rev. 114 (2013) 1909–1971.
[2] http://mcgroup.co.uk/news/20140508/china-leads-acrylic-acid-market-terms-production-consumption.html
[3] P. Lauriol-Garbey, J.M.M. Millet, S. Loridant, V. Bellière-Baca, P. Rey, J. Catal. 280 (2011) 68.
[4] P. Lauriol-Garbey, G. Postole, S. Loridant, A. Auroux, V. Belliere-Baca, P. Rey, J.M.M. Millet, Appl. Catal. B 106 (2011) 94–102.
[5] R. Znaiguia, L. Brandhorst, N. Christin, V. Bellière Baca, P. Rey, J.-M.M. Millet, S. Loridant, Micropor. Mesopor. Mater. 196 (2014) 97–103.

[6] M.A. Abdel-Rahman, Y. Tashiro, T. Zendo, K. Sonomoto, J. Biotech. 150 (Supplement) (2010) 347–348.
[7] F. Auneau, L.S. Arani, M. Besson, L. Djakovitch, C. Michel, F. Delbecq, P. Sautet, C. Pinel, Top. Catal. 55 (2012) 474–479.
[8] Y. Fan, C. Zhou, X. Zhu, Catal. Rev. 51 (2009) 293–324.
[9] C.M. Tang, J.S. Peng, X.L. Li, Z.J. Zhai, W. Bai, N. Jiang, H.J. Gao, Y.W. Liao, Green Chem. 17 (2014) 1159–1166.
[10] Z.J. Zhai, X.L. Li, C.M. Tang, J.S. Peng, N. Jiang, W. Bai, H.J. Gao, Y.W. Liao, Ind. Eng. Chem. Res. 53 (2014) 10318–10327.
[11] J. Yan, D. Yu, P. Sun, H. Huang, Chin. J. Catal. 32 (2011) 405–411.
[12] P. Sun, D. Yu, K. Fu, M. Gu, Y. Wang, H. Huang, H. Ying, Catal. Commun. 10 (2009) 1345–1349.
[13] P. Sun, D. Yu, Z. Tang, H. Li, H. Huang, Ind. Eng. Chem. Res. 49 (19) (2010) 9082–9087.
[14] J. Zhang, Y. Zhao, M. Pan, X. Feng, W. Ji, C.-T. Au, ACS Catal. 1 (1) (2011) 32–41.
[15] B. Yan, L.-Z. Tao, Y. Liang, B.-Q. Xu, ChemSusChem 7 (6) (2014) 1568–1578.
[16] J. Zhang, Y. Zhao, X. Feng, M. Pan, J. Zhao, W. Ji, C.-T. Au, Catal. Sci. Technol. 4 (5) (2014) 1376–1385.
[17] J.S. Peng, X.L. Li, C.M. Tang, W. Bai, Green Chem. 16 (2014) 108–111.
[18] J.H. Hong, J.-M. Lee, H. Kim, Y.K. Hwang, J.-S. Chang, S.B. Halligudi, Y.-H. Han, Appl. Catal. A 396 (2011) 194–2000.
[19] V.C. Ghantani, M.K. Dongare, S.B. Umbarkar, RSC Adv. 4 (2014) 33319–33326.
[20] C. Tang, J. Peng, G. Fan, X. Li, X. Pu, W. Bai, Catal. Commun. 43 (2014) 231–234.
[21] E. Blanco, P. Delichere, J.M.M. Millet, S. Loridant, Catal. Today 226 (2014) 185–191.
[22] V.C. Ghantani, S.T. Lomate, M.K. Dongare, S.B. Umbarkar, Green Chem. 15 (2013) 1211–1217.
[23] B. Yan, L.-Z. Tao, Y. Liang, B.-Q. Xu, ACS Catal. 4 (6) (2014) 1931–1943.
[24] Y. Matsuura, A. Onda, S. Ogo, K. Yanagisawa, Catal. Today 226 (2014) 192–197.
[25] Z. Zhang, Y. Qu, S. Wang, J. Wang, Ind. Eng. Chem. Res. 48 (2009) 9083–9089.
[26] P.C. Walkup, C.A. Rohrmann, R.T. Hallen, D.E. Eakin, WO 1,991 1991,011,527, 1991 A2 1991 0808.
[27] M. Hohwy, H.J. Jakobsen, M. Edén, M.H. Levitt, N.C. Nielsen, J. Chem. Phys. 108 (1998) 2686.
[28] A. Lebugle, B. Sallek, A. Tai Tai, J. Mater. Chem. 9 (1999) 2511–2515.
[29] A. Boyd, M. Akay, B.J. Meenan, Surf. Interface Anal. 35 (2003) 188.
[30] Y. Li, P.-C. Su, L.M. Wong, S. Wang, J. Power Sources 268 (2014) 804–809.
[31] D. Aurbach, I. Weissman, A. Schechter, H. Cohen, Langmuir 12 (1996) 3991–4007.
[32] R.M. Wenslow, K.T. Mueller, J. Phys. Chem. B 102 (1998) 9033–9038.
[33] Q. Wang, Q. Wang, J. Wang, X. Zhang, X. Yu, C. Wan, Mater. Res. 12 (2009) 495–501.
[34] J.C. Elliott, Studies in Inorganic Chemistry Volume 18: Structure and Chemistry of the Apatites and other Calcium Orthophosphates, Elsevier, Amsterdam-London-New York-Tokyo, 1994.
[35] R.M. Wilson, J.C. Elliott, S.E.P. Dowker, L.M. Rodriguez-Lorenzo, Biomaterials 26 (2005) 1317–1327.
[36] B. Louati, F. Hlel, K. Guidara, M. Gargouri, J. Alloys Compd. 394 (2005) 13–18.
[37] Y.-H. Tseng, J. Zhan, K.S.K. Lin, C.-Y. Mou, J.C.C. Chan, Solid State Nucl. Magn. Reson. 26 (2004) 99–104.
[38] S.J. Joris, C.H. Amberg, J. Phys. Chem. 75 (1971) 3172–3178.
[39] Z.H. Cheng, A. Yasukawa, K. Kandori, T. Ishikawa, J. Chem. Soc. Faraday Trans. 94 (1998) 1501–1505.
[40] S. Diallo-Garcia, M. Ben Osman, J.-M. Krafft, S. Boujday, G. Costentin, Catal. Today 226 (2014) 81–88.
[41] S. Diallo-Garcia, M.B. Osman, J.-M. Krafft, S. Casale, C. Thomas, J. Kubo, G. Costentin, J. Phys. Chem. C 118 (24) (2014) 12744–12757.
[42] M. Trchova, P. Capkova, P. Matejka, K. Melanova, L. Benes, J. Solid State Chem. 145 (1999) 1–9.
[43] J. Xu, D.F.R. Gilson, I.S. Butler, Spectrochim. Acta Part A 54 (1998) 1869–1878.
[44] V. Koleva, V. Stefov, A. Cahil, M. Najdoski, B. Soptrajanov, B. Engelen, H.D. Lutz, J. Mol. Struct. 919 (2009) 164–169.
[45] R.L. Frost, Y. Xi, S.J. Palmer, K. Tan, G.J. Millar, J. Mol. Struct. 1011 (2012) 128–133.
[46] R.L. Frost, S.J. Palmer, Y. Xi, Spectrochim. Acta Part A 82 (2011) 132–136.
[47] J.M. Lewis, R.A. Kydd, J. Catal. 132 (1991) 465–471.
[48] Y. Sakhno, L. Bertinetti, M. Iafisco, A. Tampieri, N. Roveri, G. Martra, J. Phys. Chem. C 114 (2010) 16640–16648.
[49] D.C. Wadley, M.S. Tam, P.B. Kokitkar, J.E. Jackson, D.J. Miller, J. Catal. 165 (1997) 162–171.
[50] http://orgchem.colorado.edu/Spectroscopy/specttutor/irchart.pdf
[51] B. Wang, C. Li, Q. Zhu, T. Tan, RSC Adv. 4 (2014) 45679–45686.
[52] U. Bentrup, A. Martin, B. Lücke, Top. Catal. 11/12 (2000) 139–145.
[53] U. Bentrup, A. Brückner, A. Martin, B. Lücke, J. Mol. Catal. A 162 (2000) 391–399.